International Journal of Dynamics and Control (2023) 11:759–770
https://doi.org/10.1007/s40435-022-01015-2

A robust estimation and compensation-based fault-tolerant control for large-scale interconnected systems with actuator saturation

Noor Safaa Abdul-Jaleel[1] · **Montadher Sami Shaker**[1]

Received: 31 May 2022 / Revised: 9 July 2022 / Accepted: 19 July 2022 / Published online: 9 August 2022

Abstract
This paper provides a robust approach for controlling large-scale interconnected nonlinear systems under actuator fault and saturation. Preserving closed-loop robustness despite the simultaneous effects of subsystem interactions, faults, and perturbations is the main challenge in such systems. Additionally, tackling the actuator saturation constraint increases the robustness challenge that must be accounted for when designing a controller for the mentioned system. Thus, the main contribution of this paper is the development of a fault-tolerant control for nonlinear interconnected systems under actuator saturation. In this framework, the proposal employs sliding mode control, control allocation, and fault estimation/compensation methodologies to ensure robust closed-loop performance. An augmented unknown input observer is utilized to simultaneously attain a robust estimation for the fault and state signals. Subsequently, the control allocation technique is used to re-locate the control signals across the residual actuators when a failure or fault occurs. The Lyapunov analysis and the linear matrix inequality were used to formulate the design. Finally, the three-degrees of freedom helicopter model are applied to satisfy the effectiveness of the proposed strategy.

Keywords Saturation · Unknown input observer · Sliding mode control · Control allocation · Fault-tolerant control

1 Introduction

With the rapid advancement of technology, the demand for a system's reliability and safety under fault scenarios is an evident and critical issue [1], especially for large-scale systems (LSS), which are complicated high-dimensional systems containing coupling, nonlinearity, and uncertainty. External disturbance and interconnection during operation are additional difficulties that increase the probability of system failure. Therefore, developing and maintaining interconnected systems with reliable control are not straightforward [2]. There are three basic control mechanisms for LSS: centralized, decentralized, and distributed control. Researchers are particularly interested in decentralized control since each subsystem relies on local information without sharing it with other subsystems. Numerous studies are concerned with decentralizing LSS [3–5]. In most practical applications for interconnected systems, components or subsystems can suddenly fail or break down, making the whole system unstable or malfunctioning [6–8]. Fault-tolerant control (FTC) is a system which automatically compensates for potential faults to ensure the entire system remains stable while providing the desired performance [9, 10]. Due to the complexity of nonlinear systems, recent research has focused on the methods that tackle the nonlinearity of the FTC system, especially for interconnected nonlinear systems; for example, the issue of decentralized adaptive tracking with actuator faults and strong interconnections is presented in [11]. In [12], a decentralized predictor control is studied, which suffers from input delay and weakly interconnections between subsystems. In [13], a fuzzy decentralized FTC with unmodeled dynamics affected by actuator faults and disturbances is discussed with unknown time delay. Fault diagnosis is the most traditional method for acquiring fault information that relies on residual signals.

In contrast, fault estimation (FE) provides essential information directly involving faults' size, time occurrence, and location without complex procedures. Research has yielded significant advances in the field of FE design based on state observers like the adaptive observer (AO) [14], the extended state observer (ESO) [15], and the sliding mode observer

✉ Noor Safaa Abdul-Jaleel
eee.19.17@grad.uotechnology.edu.iq

[1] Department of Electrical Engineering, The University of Technology, Baghdad, Iraq

(SMO) [16]. Although the methods mentioned above are effective for fault estimation, the unknown input observer (UIO) ability to entirely decouple disturbances makes it an ideal architecture for FE [9]. UIO is created in this article to simultaneously estimate the fault and state, where the estimated signals are used to compensate for faults, hence achieving overall system stability. The robustness problem of the interactions between the FE and FTC was recently described in detail by Lan and Patton [17]. This strategy has been extended to encompass a variety of applications [18–20].

Faults increase the effort of the actuator to counteract undesirable consequences, increasing the probability of actuator saturation [21]. However, this critical topic has paid less emphasis on the FE/FTC approach, particularly when the system suffers from disturbances and uncertainty [14]. Saturation of actuators is inevitable in LSS, impairing the closed-loop system's performance and stability. So, it is essential to study the control of LSS with actuator saturation to avoid this issue. Numerous noteworthy findings concerning actuator saturation in control systems were published [22, 23]. The author in [23] proposed a decentralized non-fragile control against actuator faults and saturation. An optimization method that uses convexity based on linear matrix inequalities (LMI) formulation is employed to study bounded disturbances and actuator saturation [24]. A model predictive control (MPC) is presented in [25], but none of the previous studies mention using the FTC system.

On the other hand, a strategy of an adaptive FTC with a nonlinear system subjected to actuator fault with external disturbance and actuator saturation based on sliding mode control (SMC) with radial neural network technique is discussed in [26]. A surface with a fixed time sliding mode is created to compensate for a malfunctioning spaceship attitude system to guarantee closed-loop stability [27]. In [28], the FTC is used to handle the problem of actuator saturation, assuming that the effectiveness of the actuator loss should be constant. However, none of the mentioned research used these techniques with LSS. This fact motivates the paper to propose a new strategy based on the integration design of FE/FTC for interconnected LSS with actuator faults, saturation, external disturbance, and nonlinear interactions. The combination of the SMC with the control allocation (CA) is applied to design the FTC scheme, where the virtual control signals are converted into physical actuator requirements via the CA scheme. At the same time, virtual controllers rely on the UIO, which is developed to estimate the fault. The main contributions of this paper are:

1. Compared with previous studies, this work addresses the problem of saturation level within the framework of FE and compensation-based FTC for nonlinear interconnected LSS.
2. A new strategy combining SMC, CA, and UIO is presented based on the integration technique of FE/FTC for nonlinear interconnected LSS under actuator saturation, actuator faults, external disturbance, and nonlinear interactions. Both the controller and observer gains can be obtained concurrently through a technique of LMI.

The paper is structured as follows: The FTC scheme includes the UIO-based FE with sliding mode control allocation is presented in Sect. 2. The integrated strategy of FE/FTC is proposed in Sect. 3. The simulation results are illustrated by applying a 3-DOF helicopter model in Sect. 4. Finally, Sect. 5 discusses the conclusion of the suggested approach.

2 The proposed design of FTC based on FE

The nonlinear interconnected system for the *i*th subsystem is presented as follows:

$$\begin{aligned} \dot{x}_i &= A_i x_i + B_i u_i + f_i(x_i, t) + h_i(x_i, t) + D_i d_i \\ y_i &= C_i x_i \end{aligned} \tag{1}$$

where $x_i \in R^{in}$, $y_i \in R^{ir}$, and d_i are the state, output, and external disturbance, respectively. The $A_i \in R^{in\times in}$, $B_i \in R^{in\times im}$, $C_i \in R^{ip\times in}$, and $D_i \in R^{ip\times iq}$ are constant matrices. $f_i(x_i, t) \in R^{in}$ and $\mathrm{h}_i(x_i, t) \in R^{in}$ represent the nonlinear term and nonlinear interaction, respectively.

As shown in Fig. 1, the control input applied to the system can be described as:

$$u_i^{\mathrm{sat}} = \mathrm{sat}\left(u_i^* + f_{ai}\right) \quad , i = 1, 2, \ldots, n \tag{2}$$

where u_i^* represents the design control input, f_{ai} is the actuator fault, and sat : $R^{im} \rightarrow R^{im}$ represent the standard saturation function, where sat(.) can be described as:

$$\mathrm{sat}(\Lambda_i) = \begin{cases} \mathrm{sign}(\Lambda_i) u_{i\max} & |\Lambda_i| \geq u_{i\max} \\ \Lambda_i & |\Lambda_i| < u_{i\max} \end{cases} \tag{3}$$

where $\Lambda_i = u_i^* + f_{ai}$ and $u_{\max}$ is the maximum voltage of the actuator, respectively.

Substitute the control input in (1) as:

$$u_i = u_i^* + f_{ai}^* \tag{4}$$

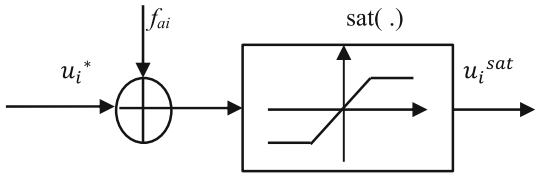

Fig. 1 The model of the actuator with fault and saturation

where f_{ai}^* represents the actuator fault influenced by the saturation, which is described as:

$$f_{ai}^* = \text{sat}\left(u_i^* + f_{ai}\right) - u_i^* \tag{5}$$

Due to the intervention of the saturation function, which is well known as non-differential, the composite fault f_{ai}^* represents the actuator fault influenced by the saturation and is non-differentiable, leading to theoretical challenges for subsequent design work of fault estimation. So, to tackle this problem, the saturation function is approximated as in (6):

$$\overline{\text{sat}}(\Lambda_i) = \begin{cases} \Lambda_i & 0 \le |\Lambda_i| \le u_{i\max} \\ \Lambda_i - \frac{\left[\Lambda_i - u_{i\max}\text{sign}(\Lambda_i)\right]^2 \text{sign}(\Lambda_i)}{2\delta_i} & u_{i\max} \le |\Lambda_i| \le u_{i\max} + \delta_i \\ \left(u_{i\max} + \frac{\delta_i}{2}\right)\text{sign}(\Lambda_i) & |\Lambda_i| \ge u_{i\max} + \delta_i \end{cases} \tag{6}$$

where δ_i is a constant, and $\overline{\text{sat}}(\Lambda_i)$ is a new function that is differentiable with constrained estimation error, which can be restricted further by choosing a suitably small δ_i.

Remark 1 Different approaches have been utilized to approximate the saturation function in the literature [29, 30]. However, the approximation in [17] is considered in this work.

The new control input described in (4) can be written as:

$$\begin{aligned} u_i &= u_i^* + f_{ai}^* + \Delta u_i \\ f_{ai}^* &= \overline{\text{sat}}\left(u_i^* + f_{ai}\right) - u_i^* \\ \Delta u_i &= \text{sat}\left(u_i^* + f_{ai}\right) - \overline{\text{sat}}\left(u_i^* + f_{ai}\right) \end{aligned} \tag{7}$$

This study includes the following assumptions:

Assumption 1 Assuming that the pair (A_i, C_i) is observable, and the pair (A_i, B_i) is controllable for $(i = 1,2,\ldots,n)$.

Assumption 2 Assume that $fi\ (xi,t)$ achieves the Lipschitz constant as follows:

$$f_i\left(\hat{x}_i, t\right) - f_i(x_i, t) \le L_f \hat{x}_i - x_i, \tag{8}$$

where L_f denotes the Lipschitz constant.

Assumption 3 The interaction $h_i(x_i, t)$ achieves:

$$h_i^T(x_i, t) h_i(x_i, t) \le \sigma_i x_i^T H_{oi}^T H_{oi} x_i, \tag{9}$$

where the σ_i indicates the positive scalar, which denotes the uncertain interaction bound; H_{oi} is a constant matrix. For the overall system, (9) can be rewritten as follows:

$$h^T(x, t) h(x, t) \le x^T H_o^T H_o x, \tag{10}$$

where $h(x, t) = [h_1(x_i, t), \ldots, h_n(x_n, t)]$ aggregates the interaction for the overall interconnected system where $H_o = \left[\sqrt{\sigma_i} H_{o1}^T, \ldots, \sqrt{\sigma_n} H_{0n}^T\right]$.

Assumption 4 It is presumed that the actuator's usable control is restricted by:

$$|u_i| \le u_{\max} \quad \text{for } (i = 1, 2, \ldots, n) \tag{11}$$

in which all actuators have the same saturation value of $u_{\max}$.

From Fig. 2, SMC is an attractive choice for designing FTC due to its inherent advantages against uncertainties. Since actuator faults can be modeled as matched uncertainty, the SMC approach "naturally" handles actuator faults from an FTC perspective. If the actuator fails to operate as required, it cannot respond to control signals; therefore, redundant actuators are essential [31]. With CA, redundant control effectors can be used efficiently to create fault tolerance without changing the underlying control rule, where the control effect is equally distributed among the actuators.

As a result of CA's flexibility, the underlying "virtual" effort can be established using any applicable control approach; therefore, CA is considered a robust candidate to be integrated with SMC to address actuator fault and saturation.

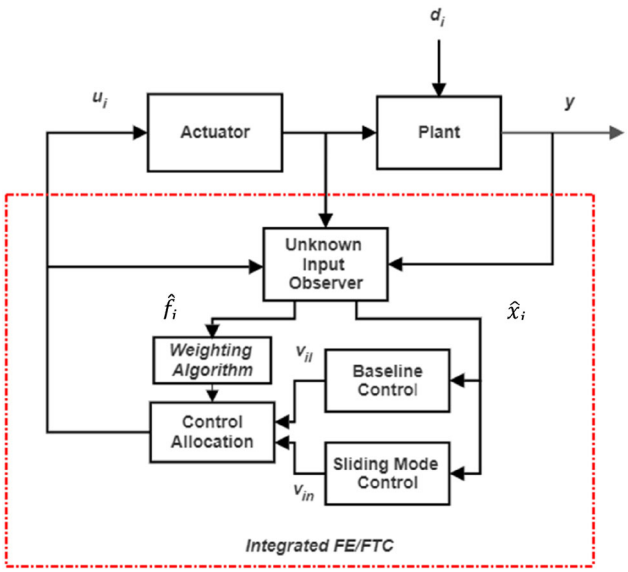

Fig. 2 The block diagram of the suggested strategy, including the design of the observer and FTC system

The following subsections discuss the method for developing decentralized SMC allocation for nonlinear LSS to accomplish the goal.

2.1 Control allocation (CA)

FTC researchers are interested in CA because it can tolerate actuator faults or failures without modifying the law of baseline control [32]. When the fault occurs, the control allocation unit redistributes control signals to the healthy one depending on their effectiveness level without changing the controller. Consider the system in (1) with redundant actuators to gain a better understanding of how the CA approach works by assuming that the distributed matrix B_i can be analyzed into two components:

$$B_i = \mathrm{B}_{iv}\mathrm{B}_{iu} \tag{12}$$

$$\text{Let } v_i = B_{iu}u_i \tag{13}$$

where v_i is the virtual control effort. According to (13), the control input can rewrite as:

$$u_i = B_{iu}^{\dagger,W} v_i \tag{14}$$

where $B_{iu}^{\dagger,W}$ represents the weighted of the right pseudo-inverse of B_{iu}, that provides some freedom to the design, which can be defined as (15), and $W = \mathrm{diag}[w_1, \ldots, w_n]$ represent the efficiency level of the actuators.

$$B_{iu}^{\dagger,W} = W B_{iu}^T \left(B_{iu} W B_{iu}^T\right)^{-1} \tag{15}$$

In case of $w_i = 1$ indicates that the *ith* actuator is operating normally with free faults. In contrast, if $1 > w_i > 0$ means that a problem is present, and the actuator is operating at a lower efficiency level, and if $w_i = 0$; this signifies that the *ith* actuator has failed and no longer responds to the control signal.

Substituting Eqs. (12)–(15) into (1) to obtain the following description of the new system:

$$\begin{aligned}\dot{x}_i &= A_i x_i + B_{iv} B_{iu}^{\dagger,W} v_i + f_i(x_i,t) + h_i(x_i,t) + D_i d_i \\ &= A_i x_i + B_{iv}\hat{v}_i + f_i(x_i,t) + h_i(x_i,t) + D_i d_i\end{aligned} \tag{16}$$

where $\hat{v}_i = B_{iu}^{\dagger,W} v_i$.

UIO is advantageous for fault estimation in over-actuated systems. With input redundancy, control can be reallocated to restrict the use of malfunctioning actuators once estimated. It is possible to integrate the CA with the FE technique to expand the number of faulty events that can be tackled, as illustrated in Sect. 2.3.

2.2 FE based on unknown input observer (UIO)

The design of UIO has gained much attention in recent decades. Unknown input decoupling is one of the most important characteristics of a UIO for state estimation in systems exposed to unknown inputs. In most practical applications, control systems are affected by unknown inputs, including external disturbances, different types of faults, etc., resulting in system performance deficiencies. This paper is motivated by the challenge of making the error signal zero despite the effect of unknown inputs, where the estimated states are asymptotically converging toward the actual states.

An augmented UIO with substituting the virtual control can illustrate as follows:

$$\begin{aligned}\dot{\overline{x}}_i &= \overline{A}_i\overline{x}_i + \overline{B}_i\hat{v}_i + \overline{f}_i(x_i,t) + \overline{h}_i(x_i,t) + \overline{D}_i\overline{d}_i \\ y_i &= \overline{C}_i\overline{x}_i\end{aligned} \tag{17}$$

where $\overline{x}_i = \begin{bmatrix} x_i \\ f_i \end{bmatrix}, \overline{A}_i = \begin{bmatrix} A_i & B_i \\ 0 & 0 \end{bmatrix}, \overline{f}_i(x_i, t) = \begin{bmatrix} f_i(x_i, t) \\ 0 \end{bmatrix}$,
$\overline{h}_i(x_i, t) = \begin{bmatrix} h_i(x_i, t) \\ 0 \end{bmatrix}, \overline{B}_i = \begin{bmatrix} B_i \\ 0 \end{bmatrix}, \overline{D}_i = \begin{bmatrix} D_i & 0 \\ 0 & I_q \end{bmatrix}$,
$\overline{d}_i = \begin{bmatrix} d_i \\ f_i \end{bmatrix}, \overline{C}_i = \begin{bmatrix} C_i & 0 \end{bmatrix}$.

The UIO can estimate the augmented state ($\overline{x}_i$) as follows:

$$\begin{aligned}\dot{z}_i &= F_i z_i + G_i\hat{v}_i + K_i y_i \\ \dot{\widehat{\overline{x}}}_i &= z_i + H_i y_i\end{aligned} \tag{18}$$

where z_i is the observer state system $\in R^{in+iq}$, and $\widehat{\overline{x}} \in R^{in+iq}$ is the estimation of $\overline{x}$. The following matrices $[F_i, G_i, T_i, K_i, \text{and} H_i]$ must be held to synthesize the UIO:

$$\left(I_{in+iq} - H_i\overline{C_i}\right)\overline{D}_i \tag{19}$$

$$T_i = I_{in+iq} - H_i\overline{C}_i \tag{20}$$

$$F_i = I_i\overline{A}_i - K_{i1}\overline{C}_i \tag{21}$$

$$G_i = T_i\overline{B}_i \tag{22}$$

$$K_{i2} = F_i H_i \tag{23}$$

$$K_i = K_{i1} + K_{i2} \tag{24}$$

$$K_i = K_{i1} + F_i H_i \tag{25}$$

The state estimation error can be determined as: $\dot{e}_i = \dot{\overline{x}}_i - \dot{\hat{\overline{x}}}_i$, and then, the dynamic error is:

$$\dot{e}_i = \left(T_i\overline{A}_i - K_{i1}\overline{C}_i\right)e_i + \left(T_i\overline{A}_i - K_{i1}\overline{C}_i - F_i\right)z_i + \left(T_i\overline{B}_i - G_i\right)\hat{v}_i + \left[\left(T_i\overline{A}_i - K_{i1}\overline{C}_i\right)H_i - K_{i2}\right]y_i + T_i\overline{f}_i(x_i,t) + T_i\overline{h}_i(x_i,t) + T_i\overline{D}_i\overline{d}_i \quad (26)$$

By substituting the matrices (19)–(25), the dynamic error becomes:

$$\dot{e}_i = \left(T_i\overline{A}_i - K_{i1}\overline{C}_i\right)e_i + T_i\overline{f}_i(x_i,t) + T_i\overline{h_i}(x_i,t) + T_i\overline{D}_i\overline{d}_i \quad (27)$$

The matrices $[F_i,\ T_i,$ and $K_{i2}]$ can be derived, while the matrices $[H_i,\ K_{i1}]$ must be determined.

Because the system under consideration is over-actuated, there remains a set of control inputs that can be used to tolerate faults. This is achieved via CA system which re-allocate control efforts from failing actuators to healthy ones if any of the actuators are prone to fault. The most frequent solution is to alter the weighting matrix (W), which relies on fault information from the fault estimation module. The greater the weighting matrix gain, the lower the control input to the associated actuator. The weighting matrix is modified based on the FE module's implying that there is no control effort transferred to a specific actuator.

The signal of the virtual control will be designed and synthesized using the SMC technique, as discussed in Sect. 2.4.

2.3 Design of sliding mode control (SMC)

The SMC is among the most potent control schemes widely used in FTC applications due to its robustness against uncertainty and disturbances [33]. To construct a sliding mode controller, there are two steps. Firstly, a sliding surface is created, upon which sliding motion will happen. The next stage is to develop a control rule that relies on the switching function and compels the system state routes to slide optimally upon the sliding surface [34, 35]. Also, the reachability requirement, which ensures the sliding mode exists on the sliding surface, is an essential criterion in the sliding mode study. In SMC theory, the selected control law is composed of two components, linear and nonlinear, designed as follows:

$$\hat{v}_i = \hat{v}_{il} + \hat{v}_{in} \quad (28)$$

where $\hat{v}_{il}$, $\hat{v}_{in}$ are linear and nonlinear components, respectively, described as:

$$\hat{v}_{il} = -K_{xi}\widehat{\overline{x}}_i \quad (29)$$

and

$$\hat{v}_{in} = -\eta_i \text{sign}(s_i), \quad (30)$$

with $\eta_i = \hat{\omega}_{si} + \varepsilon_{si}$, where ε_{si} represents the positive scaler, and $\hat{\omega}_{si}$ is an unknown scalar used to estimate of ω_{si} for each subsystem, this scalar can be updated by:

$$\dot{\hat{\omega}}_{si} = \varsigma_i s_i,\ \hat{\omega}_{si}(0) \geq 0$$

where $\varsigma_i > 0$ represents the learning rate, and s_i represents the sliding surface *which* is defined as:

$$s_i = N_i\hat{x}_i \quad (31)$$

where $N_i = B_i^+$ and $B_i^+ = (B_i^T B_i)^{-1}B_i^T$. The virtual control $\hat{v}_i$ must be determined to achieve the reachability condition for designing the SMC.

Remark 2 The rationale for using the adaptive term in Eq. (30) is to tackle the chattering and high activity control action associated with SMC. Further, adaptive approach enables designing SMC for systems with disturbance of unknown upper bound. Hence, by using Eq. 30 ($\eta_i = \hat{\omega}_{si} + \varepsilon_{si},\ \dot{\hat{\omega}}_{si} = \varsigma_i s_i,\ \hat{\omega}_{si}(0) \geq 0,\ \varsigma_i > 0$), the magnitude of the discontinuous control action becomes adaptive and can be minimized to the lowest acceptable sliding condition. Extensive explanations on adaptive SMC approaches can be found in [36, 37]

The differentiating s_i respective with time is:

$$\dot{s}_i = N_i A_i x_i + \hat{v}_i + N_i f_i(x_i,t) + N_i \text{h}_i(x_i,t) + N_i D_i d_i - N_i\dot{e}_i \quad (32)$$

Both components work together to drive the system states toward the s_i, where the appropriate selection of the s_i assists in stabilizing the system after reaching it. Assuming the Lyapunov function is:

$$V_{si} = \frac{1}{2}s_i^T s_i \quad (33)$$

and the derivative of V_{si} is:

$$\begin{aligned}\dot{V}_{si} &= s_i^T\left[N_i A_i x_i + \hat{v}_i + N_i f_i(x_i,t) + N_i h_i(x_i,t) + N_i D_i d_i - N_i\dot{e}_i\right] \\ &= s_i^T\left[N_i A_i x_i + \hat{v}_{il} + N_i f_i(x_i,t) + N_i h_i(x_i,t) + N_i D_i d_i - N_i\dot{e}_i\right] - \hat{v}_{in}]\end{aligned} \quad (34)$$

Substituting (29) and (30) in (34) gives (35):

$$\begin{aligned}\dot{V}_{si} &= s_i^T[N_i A_i x_i - K_{xi}\hat{x}_i + N_i f_i(x_i,t) + N_i h_i(x_i,t) + N_i D_i d_i - N_i\dot{e}_i] - \eta_i \text{sign}(s_i)] \\ &\leq (\Psi_{si} + \omega_{si} - \eta_i)s_i\end{aligned} \quad (35)$$

where $\Psi_{si} = N_i A_i - K_{xi}$, $\omega_{si} = N_i D_i d_i + N_i \dot{e}_i$.

After the system reaches the proposed s_i with satisfying the sliding requirement $s_1 = \dot{s}_1 = 0$, the equivalent equation is stated as:

$$\hat{v}_{\text{equ}} = -[N_i A_i x_i + N_i f_i(x_i, t) + N_i h_i(x_i, t) N_i D_i d_i] + \hat{v}_{il} \tag{36}$$

So, the system in (1) is preserved in the sliding mode with the equivalent control (36). The nonlinearity and the interactions must be reduced to ensure closed-loop robustness, which can be accomplished using the H∞ optimization described in the following section.

3 The integrated design of FE/FTC

For the overall LSS, the augmented closed-loop system can be represented as:

$$\begin{aligned} \dot{x} &= \tilde{A}x + \tilde{F}e + f(x,t) + h(x,t) \\ \dot{e} &= \tilde{A}_e e + T\overline{f}(x,t) + T\overline{h}(x,t) + T\overline{D}d \\ z &= \text{diag}[C_x x, C_e e] \end{aligned} \tag{37}$$

where

$e = [e_1, \ldots, e_n]$, $\overline{f}(x, t) = \left[\overline{f}_1(x_i, t), \ldots, \overline{f}_n(x_i, t)\right]$,

$\overline{h}(x, t) = \left[\overline{h}_1(x_i, t), \ldots, \overline{h}_n(x_i, t)\right]$, $\overline{D} = \text{diag}\left[\overline{D}_1, \ldots, \overline{D}_n\right]$,

$T = \text{diag}[T_1, \ldots., T_n]$, $\tilde{F} = \text{diag}[B_1 K_{x1} \ldots., B_n K_{xn}]$,

$\tilde{A} = \text{diag}(A_1 - B_1 K_{x1}, \ldots., A_n - B_n K_{xn})$,$\tilde{A}_e = \text{diag}\left(T_1\overline{A}_1 - K_{11}\overline{C}_1, \ldots, T_n\overline{A}_n - K_{n1}\overline{C}_n\right)$,$z \in R^{2\overline{n}+\overline{q}}$, represent the output measured that used to confirm the closed-loop system by the matrices $C_x \in R^{\overline{n}\times\overline{n}}$, and $C_e \in R^{(\overline{n}+\overline{q})\times(\overline{n}+\overline{q})}$, where, $\overline{n} = [n_1, \ldots, n_{in}]$, $\overline{q} = [q_1, \ldots q_{in}]$, respectively.

The design problem of FE and FTC can be handled through the H∞ optimization and the LMI approach, as illustrated in Theorem 1.

Theorem 1 *According to Assumptions* (1–3)*, the system is stable with the performance of H∞* $G_{z\overline{d}\infty} < \beta$, *if the following optimization is possible*:

Min $\sum_{i=1}^{n}(\mu_i + \beta_i)$, *with subject to*:

$$\begin{bmatrix} \Pi_{11} & \Pi_{12} & \Pi_{13} & 0 & \Pi_{15} & 0 & \Pi_{17} \\ * & \Pi_{22} & 0 & \Pi_{24} & 0 & \Pi_{26} & 0 \\ * & * & -\delta_3^{-1} Z & 0 & 0 & 0 & 0 \\ * & * & * & -\delta_2 Z & 0 & 0 & 0 \\ * & * & * & * & -\epsilon I & 0 & 0 \\ * & * & * & * & * & -\delta_1 I & 0 \\ * & * & * & * & * & * & -I \\ * & * & * & * & * & * & * \\ * & * & * & * & * & * & * \end{bmatrix}$$

$$\begin{bmatrix} 0 & 0 \\ \Pi_{28} & \Pi_{29} \\ 0 & 0 \\ 0 & 0 \\ 0 & 0 \\ 0 & 0 \\ 0 & 0 \\ -I & 0 \\ * & -\overline{\beta} \end{bmatrix} < 0 \tag{38}$$

where

$\in = \text{diag}(\in_1, \ldots, \in_n)$, $\mu = \text{diag}([\mu_1, \ldots, \mu_n])$, $\Pi_{11} = \text{diag}(\Pi_{111}, \ldots, \Pi_{11n})$, $\Pi_{11i} = \text{He}(A_i Z_i) + \delta_{i2}^{-1} I$, $\Pi_{12} = \text{diag}([0, F_1], .., [0, F_n])$, $\Pi_{13} = \text{diag}(B_1 M_{1i}, \ldots, B_n M_{1n})$.

$$\Pi_{15} = \begin{pmatrix} Z_1 M_{011}^T & \cdots & Z_1 M_{0n1}^T \\ \vdots & \ddots & \vdots \\ Z_n M_{01n}^T & \cdots & Z_n M_{0nn}^T \end{pmatrix}, \Pi_{17} = \begin{bmatrix} Z_1 C_{x1}^T \\ \vdots \\ Z_n C_{xn}^T \end{bmatrix},$$

$\Pi_{22} = \text{diag}(\Pi_{221}, \ldots, \Pi_{22n})$, $\Pi_{22i} = \begin{bmatrix} T_{22i} & T_{23i} \\ * & T_{33i} \end{bmatrix}$,

$T_{22i} = \text{He}(Q_{i1} A_i - M_{4i} C_i A_i - M_{2i} C_i)$,

$T_{23i} = Q_{i1} F_i - M_{4i} C_i F_i - (M_{5i} C_i A_i + M_{3i} C_i)^T$,

$T_{33i} = \text{He}(-M_{5i} C_i F_i)$, $\Pi_{24} = [0, I]$,

$\Pi_{26} = \text{diag}(Q_1 T_1, \ldots, Q_n T_n)$, $Q_i T_i = \begin{bmatrix} Q_{i1} - M_{4i} C_i & 0 \\ -M_{5i} C_i & Q_{i2} \end{bmatrix}$,

$\Pi_{28} = \begin{bmatrix} C_{e1}^T \\ \vdots \\ C_{en}^T \end{bmatrix}$, $\Pi_{29} = \text{diag}(\Pi_{291}, \ldots, \Pi_{29n})$, $\Pi_{29i} = \begin{bmatrix} 0 \\ Q_{i2} \end{bmatrix}$.

The gains of the state feedback control and the observer are:

$K_{xi} = M_{1i} Z_i^{-1}$, $K_{i11} = Q_{i1}^{-1} M_{2i}$, $K_{i12} = Q_{i1}^{-1} M_{3i}$, $H_{i1} = Q_{i1}^{-1} M_{4i}$, $H_{i2} = Q_{i2}^{-1} M_{5i}$

Proof Consider the Lyapunov functions with s.p.d P and Q matrices:

$V_1 = e^T P$ e and $V_2 = x^T Q$x.

The time derivative of V_1 concerning (37) is:

$$\begin{aligned}\dot{V}_1 &= e^T P\dot{e} + \dot{e}^T Pe \\ &= e^T P\left[\tilde{A}_e + T\overline{f}(x,t) + T\overline{h}(x,t) + T\overline{Dd}\right] \\ &\quad + \left[\tilde{A}_e + T\overline{f}(x,t) + T\overline{h}(x,t) + T\overline{Dd}\right]^T Pe \\ &= e^T He[P\left(\tilde{A}_e\right) + \delta_1^{-1} PTT^T P + \delta_1 L_f^2 I + \alpha_1^{-1} PT \\ &\quad T^T P]e + \alpha_1 x^T H_0^T H_0 x + He\left(e^T PT\overline{Dd}\right) \\ &\leq x^T[He\left(P\tilde{A}_e\right) + \delta_1^{-1} PTT^T P + \delta_1 L_f^2 I + \alpha_1^{-1} PT \\ &\quad T^T P]e + He\left(e^T PT\overline{Dd}\right) + \alpha_1 x^T H_0 H_0^T x \end{aligned} \tag{39}$$

where δ_1 and α_1 are positive scalars, with s.p.d matrice P, the system is stable $\dot{V}_1 < 0$. □

The time derivative of V_2 is:

$$\dot{V}_2 = x^T Q\dot{x} + \dot{x}^T Qx$$

$$\begin{aligned}\dot{V}_2 &= x^T Q[\tilde{A}x + \tilde{F}e + f(x,t) + h(x,t) + D\overline{d}] \\ &\quad + \left[\tilde{A}x + \tilde{F}e + f(x,t) + h(x,t) + D\overline{d}\right]^T Qx \\ &= x^T Q\tilde{A}x + x^T Q\tilde{F}e + x^T Qf(x,t) + x^T Qh(x,t) \\ &\quad + x^T QD\overline{d} + x^T \tilde{A}^T Qx + e^T \tilde{F}^T + f(x,t)^T \\ &\quad + h(x,t)^T + x^T QHe\left(Q\tilde{A}\right)x + He\left(x^T Q\tilde{F}\right) \\ &\quad + \delta_2^{-1} x^T Q\varphi\varphi^T Qx + \delta_2 L_f^2 I + x^T \alpha_2^{-1} QQx \\ &\quad + \alpha_2 x^T H_0 H_0^T x, \\ &\leq x^T[He\left(Q\tilde{A}\right) + \delta_2^{-1} Q\varphi\varphi^T Q + \delta_2 L_f^2 \\ &\quad + \alpha_2^{-1} QQ]x + He\left(x^T Q\tilde{F}e\right) + He\left(x^T QD\overline{d}\right) \\ &\quad + \alpha_2 x^T H_0 H_0^T x, \end{aligned} \tag{40}$$

where $\varphi = I_n - BN$, and δ_2 and α_2 are some positive scalars.

Clearly, the inequalities in (39) and (40) are obtained by substituting the upper bound of Assumptions 2 and 3 in equations of $\dot{V}_1$ and $\dot{V}_2$. The closed-loop system in (37) is stable if:

$$\dot{V}_1 + \dot{V}_2 < 0, \tag{41}$$

Assuming that $\Im = \left[x^T, e^T\right]$, the H_∞ optimization can be obtained as:

$$\Omega = \int_0^\infty \left(\Im^T \Im - \mu^2 \overline{d}^T \overline{d}\right) \mathrm{d}t < 0, \tag{42}$$

with (zero) initial conditions:

$$\begin{aligned}\Omega &= \int_0^\infty \left(\Im^T \Im - \mu^2 \overline{d}^T \overline{d} + \dot{V}_1 + \dot{V}_2\right) \mathrm{d}t - \int_0^\infty \left(\dot{V}_1 + \dot{V}_2\right) \mathrm{d}t \\ &= \int_0^\infty \left(\Im^T \Im - \mu^2 \overline{d}^T \overline{d} + \dot{V}_1 + \dot{V}_2\right) \mathrm{d}t - (V_1(\infty) \\ &\quad + V_2(\infty) + V_1(0) + V_2(0)) \\ &\leq \int_0^\infty \left(\Im^T \Im - \mu^2 \overline{d}^T \overline{d} + \dot{V}_1 + \dot{V}_2\right) \mathrm{d}t, \end{aligned}$$

$$\text{Then, } \Im^T \Im - \mu^2 \overline{d}^T \overline{d} + \dot{V}_1 + \dot{V}_2 < 0 \tag{43}$$

Substituting (39) and (40) then:

$$\Omega = \begin{bmatrix} x \\ e \\ \overline{d} \end{bmatrix}^T \begin{bmatrix} \Omega_{11} & \Omega_{12} & \Omega_{13} \\ * & \Omega_{22} & \Omega_{23} \\ * & * & \Omega_{33} \end{bmatrix} \begin{bmatrix} x \\ e \\ \overline{d} \end{bmatrix} < 0 \tag{44}$$

Inequality (44) must equal to:

$$\begin{bmatrix} \Omega_{11} & \Omega_{12} & \Omega_{13} \\ * & \Omega_{22} & \Omega_{23} \\ * & * & \Omega_{33} \end{bmatrix} < 0 \tag{45}$$

where

$$\begin{aligned}\Omega_{11} &= He\left(Q\tilde{A}\right) + \delta_2^{-1} Q\varphi\varphi^T Q + \delta_2 L_f^2 I + \alpha_2^{-1} QQ^T \\ &\quad + \alpha_2 H_0 H_0^T + C_x^T C_x \Omega_{12} = \Omega_{12} = Q\tilde{F},\ \Omega_{13} = QD, \end{aligned}$$

$$\begin{aligned}\Omega_{22} &= He\left(P\tilde{A}_e\right) + \delta_1^{-1} PTT^T P + \delta_1 L_f^2 I + \alpha_1^{-1} PTT^T P \\ &\quad + C_e^T C_e,\ \Omega_{23} = PTD,\ \Omega_{33} = -\mu^2 I. \end{aligned}$$

Let $Z = P\text{-}1$, by multiplying both sides of (45) by the diagonal (Z, I, I), then (45) becomes:

$$\begin{bmatrix} \Omega_{11} & \Omega_{12} & \Omega_{13} \\ * & \Omega_{22} & \Omega_{23} \\ * & * & \Omega_{33} \end{bmatrix} < 0 \tag{46}$$

$$\begin{aligned}\Omega_{11} &= He\left(\tilde{A}Z\right) + \delta_2^{-1} \varphi\varphi^T + \delta_2 L_f^2 ZZ + \alpha_2^{-1} I \\ &\quad + \alpha_2 ZH_0 H_0^T Z + ZC_x^T C_x Z,\ \Omega_{12} = \tilde{F},\ \Omega_{13} = D, \end{aligned}$$

$$\begin{aligned}\Omega_{22} &= He\left(P\tilde{A}_e\right) + \delta_1^{-1} PTT^T P + \delta_1 L_f^2 I + \alpha_1^{-1} PTT^T P \\ &\quad + C_e^T C_e,\ \Omega_{23} = PTD,\ \Omega_{33} = -\mu^2 I. \end{aligned}$$

Remark 3 By using Schur complement theorem and after simple manipulation, the matrix inequality (38) can be easily obtained [38]. LMI toolbox can be used for obtaining the design variable that achieve negativity of (38). Hence, by satisfying Assumptions (1–3), solution of the optimization problem of Theorem 1 guarantees stability of the system with H∞ performance of $G_{z\overline{d}\infty} < \beta$.

Remark 4 It is worth mentioning that references [5, 9, 15] neither deal with the actuator saturation nor the integrated design between the fault estimation and fault-tolerant control. For instance, [5] has dealt with the class of uncertain linear interconnected systems based on the backstepping method, considering the disturbance and interconnection consist of matched and mismatched parts, using the cyclic-small-gain to handle the problem of mismatched interconnections. On the other hand, the authors in [9] have dealt with uncertain nonlinear large-scale systems, using the radial basis function neural network to approximate the unknown nonlinear interconnections. Similarly, the nonlinear system with actuator fault has been considered in [15]. Compared with the research above, the proposed control strategy has employed the sliding mode control allocation fault-tolerant control to deal with nonlinear interconnected systems affect by actuator fault, saturation, and interconnections.

4 Simulation results

A three degree of freedom (3-DOF) helicopter [39] is described in this paper in order to demonstrate the efficacy of the proposed approach (see Fig. 3), which can be briefly described as follows:

where $\epsilon(t)$, $p(t)$, and $\gamma(t)$ represent the elevation angle, pitch angle, and travel angle, respectively, and ϵ_o is the initial arm-base angle. F_f, F_b are the control voltages for the front and back motors. J_1, J_2, and J_3 are the moments of inertia that pertain to the axis of elevation, pitch, and travel; K_f is the coefficient of force-thrust between propellers; and m is the helicopter's effective mass. The gravity constant denotes by g equals 9.8 m/s2; L_a is the distance of the travel axis to the helicopter's body; L_h is the distance of the pitch axis to each motor. The mathematical model of the proposed model is [32]:

$$
\begin{aligned}
J_1\ddot{\epsilon} &= K_f L_a \cos p\left(F_f + F_b\right) - mgL_a \sin(\epsilon + \epsilon_0) + d_1\\
J_2\ddot{p} &= K_f L_h\left(F_f - F_b\right) + d_2\\
J_3\ddot{\gamma} &= K_f L_a \sin p\left(F_f + F_b\right) + d_3
\end{aligned}
\tag{47}
$$

The control system has two inputs and two outputs. Only two available control inputs are ready for control in this model: the helicopter's elevation and pitch angles. The state-space can be described as:

$$\dot{x}_{11} = x_{12}$$

$$\dot{x}_{12} = b_1 u_1$$

$$\dot{x}_{21} = x_{22}$$

$$\dot{x}_{22} = b_2 u_2$$

$$y_1 = x_{11}$$

$$y_2 = x_{21}$$

where $x^T = [x_{11}x_{12}x_{21}x_{22}] = \left[\epsilon\ \dot{\epsilon}\ p\ \dot{p}\right]$ represent the state vector, $u^T = [u_1 u_2] = \left[u_f u_b\right]$ is the vector of control inputs for front and back motors, and $y^T = [y_1 y_2] = [\epsilon\ p]$ is the output vector. The values of bi for $(i = 1, 2)$ are given by: $b_1 = \frac{K_f L_a}{J_1}\cos x_{21}$ and $b_2 = \frac{K_f L_h}{J_2}$

Remark 5 The pitch angle is limited during the interval.

$\left(\frac{-\pi}{2}, \frac{\pi}{2}\right)$ assuming that $x_{21} \in \left[\frac{-\pi}{2} + \theta_0, \frac{\pi}{2} - \theta_0\right]$, where θ_0 is a positive constant.

The helicopter's significant parameters are mentioned in Table 1.

Due to mechanical constraints, the pitch angle is limited to ± 31 degrees, the elevation angle is to ± 30.5 degrees, and the restriction of the maximum voltage is ± 0.2. According to Assumption 1, all subsystems are verified locally and globally controllable and observable. The required parameters are given as $\beta = 0.2$, $\delta_{11} = \delta_{12} = 0.01$, $\delta_{21} =$

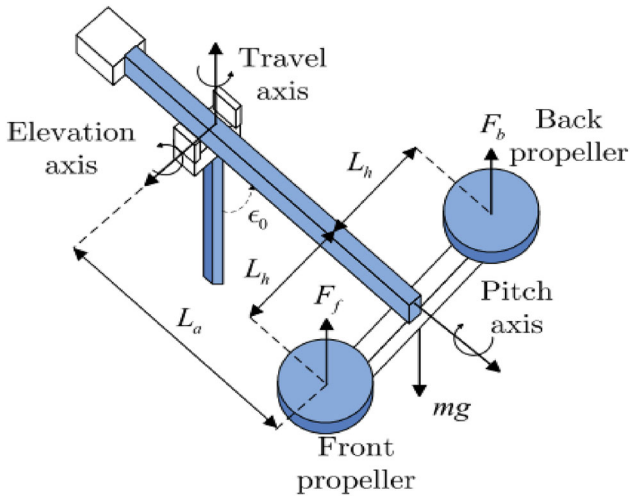

Fig. 3 The model of a 3-DOF helicopter [39]

Table 1 The parameters of a 3-DOF helicopter [39]

The parameters	The value
J_1	0.9138 kg m^2
J_2	0.0364 kg m^2
K_f	0.1188 N/V
m	1 kg
L_a	0.66 m
L_h	0.178 m

$\delta_{22} = 10$, $\alpha_1 = \alpha_2 = 10$. The integrated design is simulated based on the parameters solved by Theorem 1, which gives: $\overline{\mu}_1 = 242.031$, $\overline{\mu}_2 = 139.553$. The external disturbance $d_1 = 0.01$, and $d_2 = 0.02$, and $h_i(x_i, t) = \sum_{j=1, j\neq i}^{n} p_{ij} G_{ij} g_{ij}(x_i, x_j)$, where:

$g_{ij}(x_i, x_j) = \sin(\sigma_i - \sigma_j) - \sin(\sigma_{i0} - \sigma_{j0})$.

For the first subsystem

$$K_{x1} = \begin{bmatrix} 9.136 \\ 1.724 \end{bmatrix}, G_1 = \begin{bmatrix} 0 \\ -29.102 \\ 0 \end{bmatrix},$$

$$H_1 = \begin{bmatrix} 1 & 0 \\ 0 & 1 \\ 0.002 & 0.015 \end{bmatrix}, K_1 = \begin{bmatrix} 0 & 0 \\ 0 & 0 \\ -0.031 & -0.020 \end{bmatrix},$$

$$F_1 = \begin{bmatrix} 0.220 & -0.089 & -1.302 \\ -0.035 & 0.220 & -0.247 \\ 0 & 0.021 & -21.042 \end{bmatrix},$$

For the second subsystem

$$K_{x2} = \begin{bmatrix} 7.028 \\ 2.301 \end{bmatrix}, G_2 = \begin{bmatrix} 0 \\ -18.089 \\ 0 \end{bmatrix}, H_2 = \begin{bmatrix} 1 & 0 \\ 0 & 1 \\ 0.001 & 0 \end{bmatrix},$$

$$K_2 = \begin{bmatrix} 0 & 0 \\ 0 & 0 \\ -0.011 & -0.032 \end{bmatrix},$$

$$F_2 = \begin{bmatrix} 0.782 & -0.105 & -1.408 \\ -0.301 & 0.102 & -0.235 \\ 0 & 0.042 & -18.056 \end{bmatrix}$$

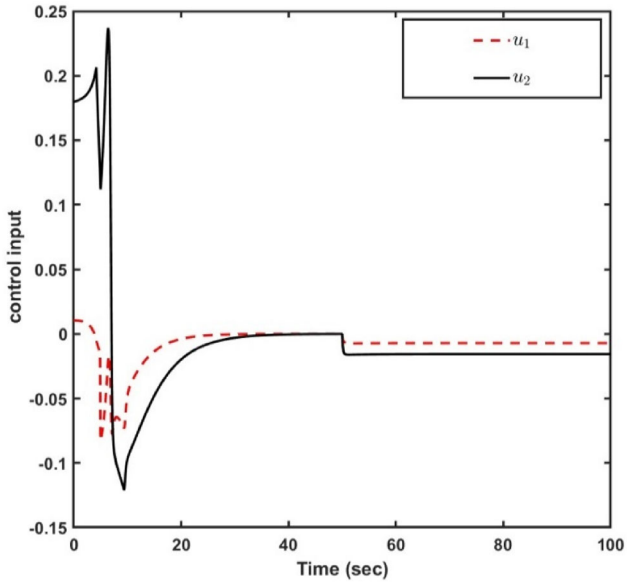

Fig. 4 The control input for each subsystem when exceeding the saturation level

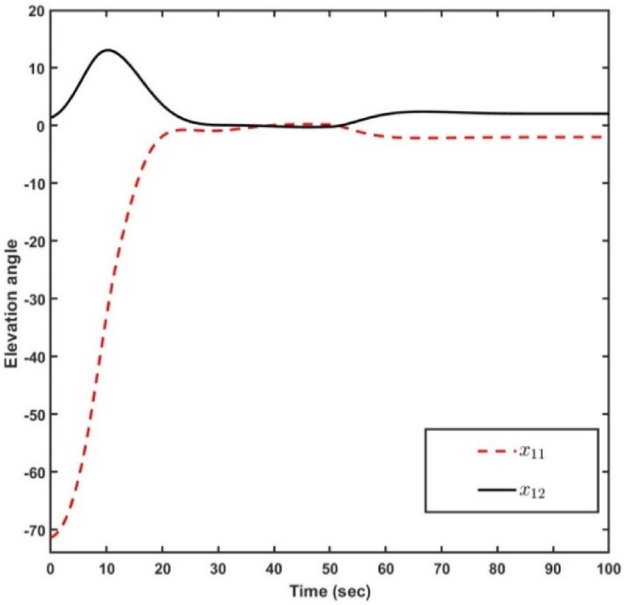

Fig. 5 The system state for the first subsystem without FTC

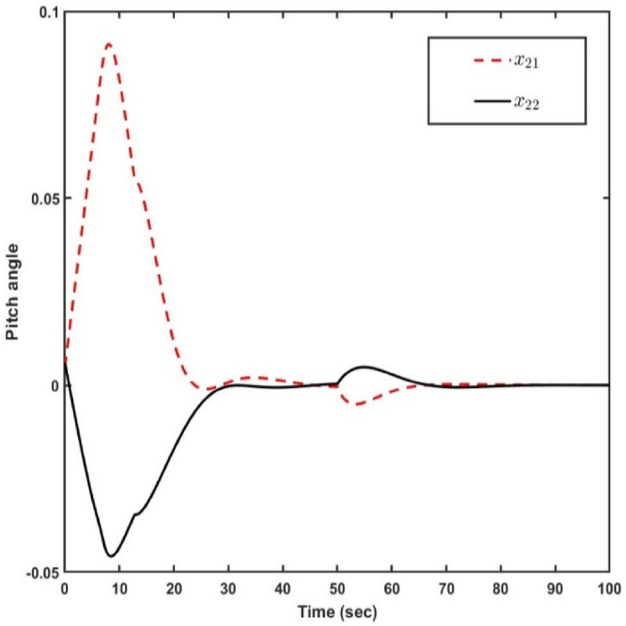

Fig. 6 The system state for the second subsystem without FTC

For the design of the FTC, the SMC is constructed when the sliding surface is obtained as:$s_i = (-0.0246 - 0.8)\hat{x}, \partial_i = \hat{\omega}_{si} + 0.8, \hat{\omega}_{si}(0) = 1$. Keeping the typical controller magnitude below 0.2 Nm to meet the actuator saturation constraint is necessary.

When adding the actuator fault to the proposed system, the performance of the control inputs, the elevation and pitch angles response for each subsystem is shown in Figs. 4, 5 and 6, respectively.

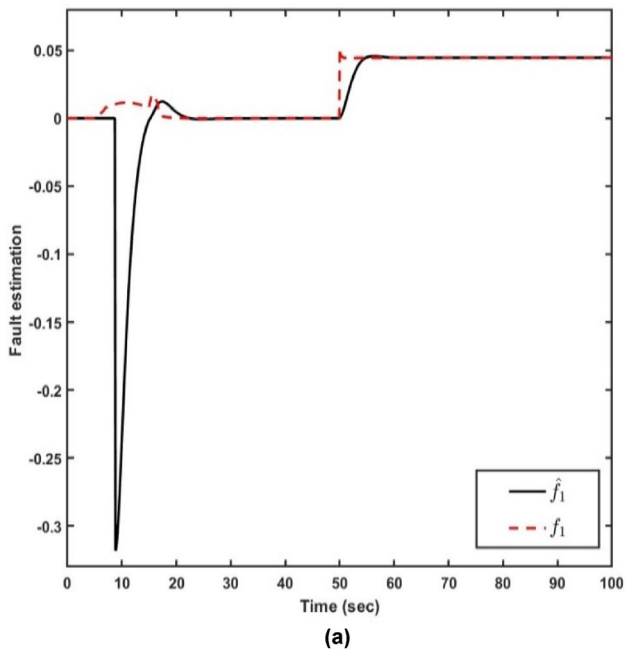

(a)

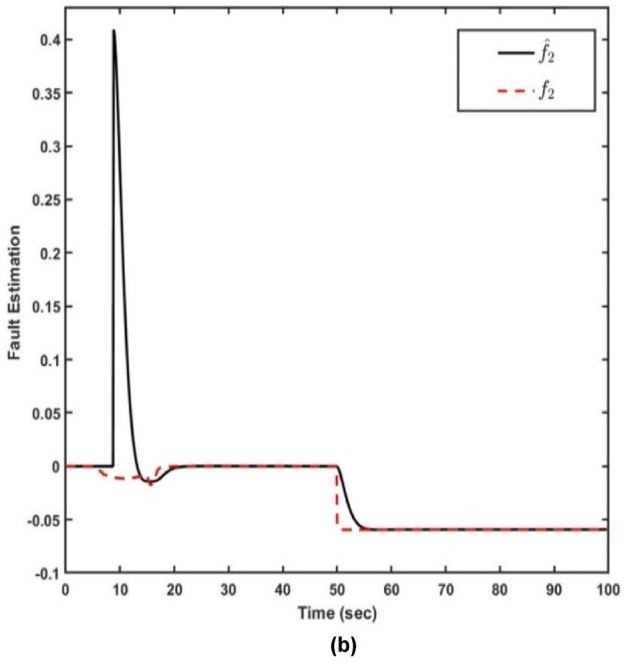

(b)

Fig. 7 Actuator faults and their estimation for: **a** the first subsystem, **b** the second subsystem

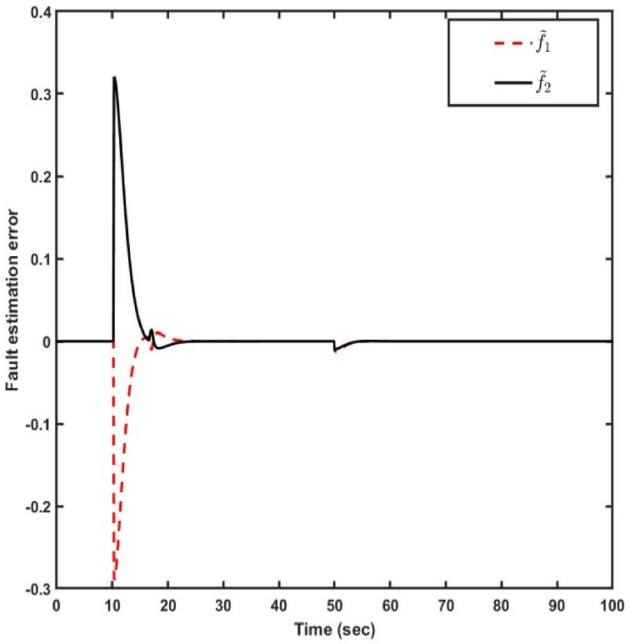

Fig. 8 Fault estimation error

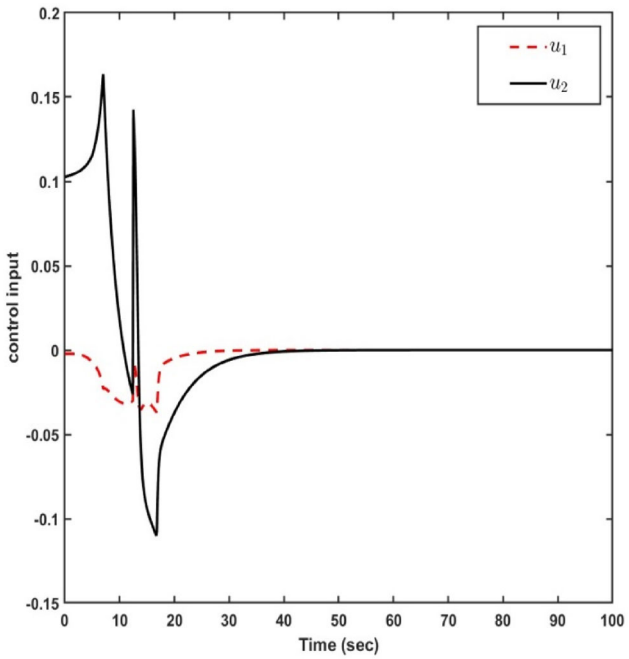

Fig. 9 The control inputs under FTC

Figure 4 illustrates the control input when the permissible value of saturation level ($u_{imax} = 0.2$) is exceeded.

Figures 5 and 6 illustrate the performance of the system states for each subsystem under nominal control; it can be noticed that the states are still stable without actuator malfunction despite some overshoot at the starting due to the disturbance and nonlinear interactions. However, they exhibit unacceptable performance once the fault occurs at 50 s.

Figure 7 shows the actuator faults simulation results and their estimation for each subsystem. It is clear that the actuator faults completely match their estimation in the first and second subsystems; in contrast, some overshoot occurs at starting. Such overshoots can be limited by modifying the performance index and the parameters of pole placement.

According to Fig. 8, the fault estimation error will eventually converge to a value around zero. We notice a small

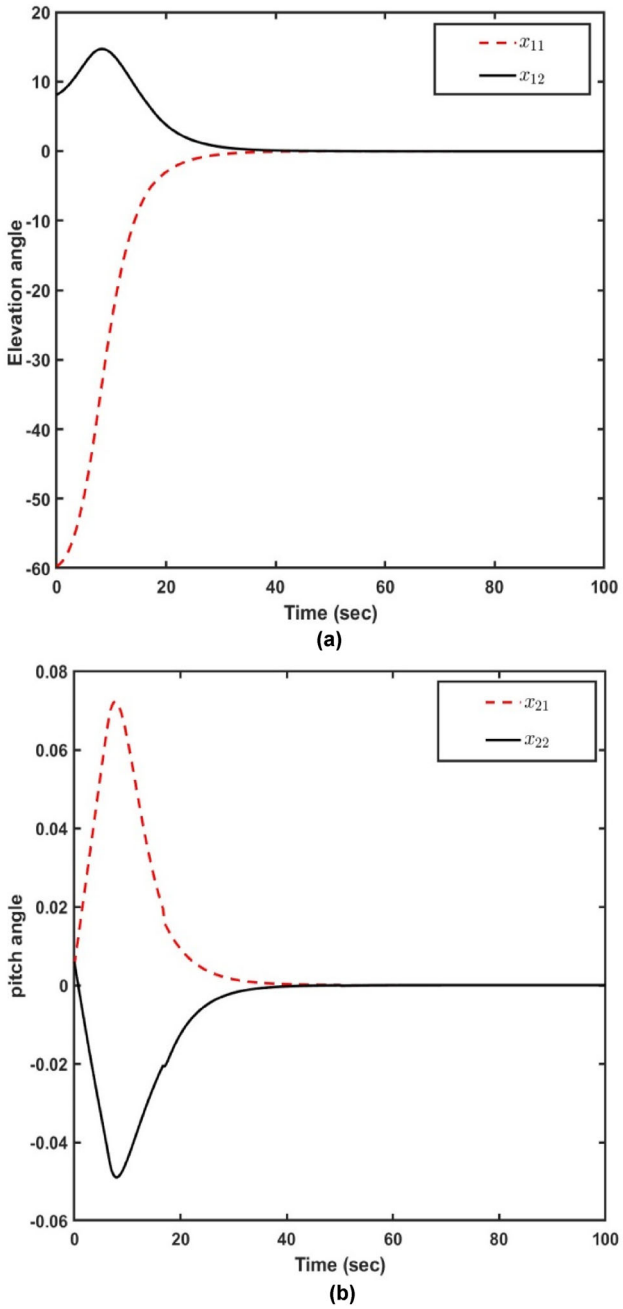

Fig. 10 The system state under FTC for: **a** the first subsystem, **b** the second subsystem

increase occurs after 50 s due to the effect of the additive fault.

The FTC system can be used to compensate for the influence of fault and maintains system stability. The control input responses, elevation and pitch angles are shown in Figs. 9 and 10, from which it may be noted that good control performance is attained. Moreover, the proposed controller has limited the control input to less than 0.2 Nm, mainly after the fault occurs.

By summarizing the simulation results, compared to the nominal approach, the integrated FE/FTC design can stabilize the proposed system with optimum performance, while avoiding the actuator saturation once a fault occurs.

5 Conclusions

This paper has presented a FTC for nonlinear interconnected systems under actuator saturation. The proposal combines the SMC, CA, and fault estimation/compensation methodologies to ensure robust closed-loop performance. The integrated approach of decentralized FE/FTC is illustrated using the 3-DOF helicopter suffering from saturation, actuator fault, nonlinear interaction, and external disturbance. In the presented framework, the problem of actuator saturation within FE/FTC has been highlighted and tackled efficiently. This has been achieved via employing the decoupling capability of SMC and UIO within integrated FE/FTC loop. Simulation results have shown the sliding mode FTC allocation technique efficacy in compensating for the hard effect of saturation and actuator fault, thereby achieving the stability of the whole system.

Authors contributions NSAJ wrote the manuscript and provided the simulation results, and MSS provided data. All authors reviewed the final manuscript.

Funding No funding was received.

Declarations

Conflict of interest We declare that there are no conflicts of interest.

References

1. Zhao B, Wang D, Shi G, Liu D, Li Y (2018) Decentralized control for large-scale nonlinear systems with unknown mismatched interconnections via policy iteration. IEEE Trans Syst Man Cybern Syst 48(10):1725–1735. https://doi.org/10.1109/TSMC.2017.2690665
2. Zhou S, Bai J, Wu F (2021) Decentralized fault detection and fault-tolerant control for nonlinear interconnected systems. Processes 9(4):1–17. https://doi.org/10.3390/pr9040591
3. He W, Li S, Ahn CK, Guo J, Xiang Z (2021) Global decentralized control of p-normal large-scale nonlinear systems based on sampled-data output feedback. IEEE Syst J 15(3):3540–3548. https://doi.org/10.1109/JSYST.2020.2997029
4. Sarbaz M, Zamani I, Manthouri M, Ibeas A (2022) Decentralized robust interval type-2 fuzzy model predictive control for Takagi-Sugeno large-scale systems. Automatika 63:49–63. https://doi.org/10.1080/00051144.2021.2003113
5. Xie CH, Yang G (2017) Decentralized adaptive fault-tolerant control for large-scale systems with external disturbances and actuator faults. Automatica 85:83–90. https://doi.org/10.1016/j.automatica.2017.07.037

6. Vu V, Wamg WJ (2021) Decentralized observer-based controller synthesis for a large-scale polynomial T-S fuzzy system with nonlinear interconnection terms. IEEE Trans Cybern 51:3312–3324. https://doi.org/10.1109/TCYB.2019.2948647
7. Lee TH, Lim CP, Nahavandi S, Roberts RG (2019) Observer-based H∞ fault-tolerant control for linear systems with sensor and actuator faults. IEEE Syst J 13:1981–1990. https://doi.org/10.1109/JSYST.2018.2800710
8. Yang H, Jiang B, Staroswiecki M, Zhang Y (2015) Fault recoverability and fault tolerant control for a class of interconnected nonlinear systems. Automatica 54:49–55. https://doi.org/10.1016/j.automatica.2015
9. Chen M, Tao G (2016) Adaptive fault-tolerant control of uncertain nonlinear large-scale systems with an unknown dead zone. IEEE Trans Cybern 46:1–12. https://doi.org/10.1109/TCYB.2015.2456028
10. Torabi N, Motavalli MR, Mihankhah A, Rastani S (2021) Fault tolerant sliding mode intelligent control based on fault hiding for a nonlinear induction furnace system. Int J Dyn Control 9:636–644. https://doi.org/10.1007/s40435-020-00672-5
11. Wang P, Yu C, Sun J (2021) Decentralized adap- tive tracking control for nonlinear large-scale systems with unknown control directions. Int J Robust Nonlinear Control 22:620–648. https://doi.org/10.1002/rnc.5843
12. Zhu Y, Fridman E (2020) Predictor methods for decentralized control of large-scale systems with input delays. Automatica 116:1–9. https://doi.org/10.1016/j.automatica.2020.108903
13. Moradvandi A, Shahrokhi M, Malek SA (2019) Adaptive fuzzy decentralized control for a class of MIMO large-scale nonlinear state delay systems with unmodeled dynamics subject to unknown input saturation and infinite number of actuator failures. Inf Sci 475:121–141. https://doi.org/10.1016/j.ins.2018.09.052
14. Tong S, Huo B, Li Y (2014) Observer-based adaptive decentralized fuzzy fault-tolerant control of nonlinear large-scale systems with actuator failures. IEEE Trans Fuzzy Syst 22:1–15
15. Hadi A, Shaker M (2020) A new estimation/decoupling approach for robust observer-based fault reconstruction in nonlinear systems affected by simultaneous time-varying actuator and sensor faults. J Franklin Inst 357(13):8956–8979
16. Farahani AV, Abolfathi S (2021) Sliding Mode Observer Design for decentralized multi-phase flow estimation. Heliyon 8(2):e08768
17. Lan J, Patton RJ, Zhu X (2017) Integrated fault-tolerant control for a 3-DOF helicopter with actuator faults and saturation. IET Control Theory Appl 11(14):2232–2241
18. Lan J, Patton RJ (2017) Integrated design of fault-tolerant control for nonlinear systems based on fault estimation and T-S fuzzy modeling. IEEE Trans Fuzzy Syst 25(5):1141–1154
19. Wang YK, Wang JS (2016) Optimization of PID controller based on PSO-BFO algorithm. In: Proceedings of 28th Chinese Control Decis. Conf. CCDC, Yinchuan, China
20. Guna G, Prabhakaran D, Thirumarimurugan M (2021) Design, implementation, control and optimization of single stage pilot scale reverse osmosis process. Water Sci Technol 84(10–11):2923–2942
21. Senpagam S, Dhanalakshmi P, Mohanapriya R (2022) Fault tracking sliding-mode controller design for fuzzy fractional-order system subject to actuator saturation. Int J Dyn Control 10:270–282. https://doi.org/10.1007/s40435-021-00794-4
22. Li H, Wang J, Shi P (2016) Output-feedback based sliding mode control for fuzzy systems with actuator saturation. IEEE Trans Fuzzy Syst 24:1282–1293
23. Zhao L, Xu H, Yuan Y, Yang H (2017) Stabilization for networked control systems subject to actuator saturation and network-induced delays. Neurocomputing 267:354–361
24. Deng C, Yang GH (2017) Consensus of linear multi-agent systems with actuator saturation and external disturbances. IEEE Trans Circuits Syst II: Express Br 64:284–288
25. Peng H, Li F, Zhang S, Chen B (2017) A novel fast model predictive control with actuator saturation for large-scale structures. Comput Struct 187(23–24):35–49. https://doi.org/10.1016/j.compstruc.2017.03.014
26. Qian M, Zheng Z, Gheng P (2019) Adaptive NFTSM-based fault tolerant control for a class of nonlinear system with actuator fault and saturation. IEEE Access 7:107083–107095. https://doi.org/10.1109/ACCESS.2019.2932275
27. Jiang B, Hu Q, Friswell MI (2016) Fixed-time attitude control for rigid spacecraft with actuator saturation and faults. IEEE Trans Control Syst Technol 24(5):1892–1898
28. Shen Q, Yue C, Wang D, Goh CH (2019) Active fault-tolerant control system design for spacecraft attitude maneuvers with actuator saturation and faults. IEEE Trans Ind Electron 66(5):3763–3772. https://doi.org/10.1109/TIE.2018.2854602
29. Hamzeh A, Alireza A (2020) Design of adaptive robust controller for second-order non-affine systems with input saturation. J Control Autom Electr Syst 31:535–547
30. Mojtaba H, Ali K, Mahyar N, Chee P (2019) (2019) Saturated fault tolerant control based on partially decoupled unknown-input observer: a new integrated design strategy. IET Control Theory Appl 13:2104–2113
31. Castro R, Brembeck J (2021) Lyapunov-based fault tolerant control allocation. Veh Syst Dyn. https://doi.org/10.1080/00423114.2021.1971265
32. Mashud A, Bera MK (2021) Control allocation based fault tolerant control of descriptor system with actuator saturation. ISA Trans. https://doi.org/10.1016/j.isatra.2021.12.028
33. Gambhire SJ, Kishore DR, Londhe PS et al (2021) Review of sliding mode based control techniques for control system applications. Int J Dyn Control 9:363–378
34. Hadi A, Shaker M (2019) Estimation/decoupling approach for robust Takagi-Sugeno UIO-based fault reconstruction in nonlinear systems affected by a simultaneous time-varying actuator and sensor faults. Int J Syst Sci 50(13):2473–2485. https://doi.org/10.1080/00207721.2019.1671528
35. Shaker M, Kraidi A (2017) Robust fault-tolerant control of wind turbine systems against actuator and sensor faults. Arab J Sci Eng 42(7):3055–3063. https://doi.org/10.1007/s40435-020-00638-7
36. Utkin VI, Poznyak AS (2013) Adaptive sliding mode control. In: Bandyopadhyay B, Janardhanan S, Spurgeon S (eds) Advances in sliding mode control. Lecture notes in control and information sciences, vol 440. Springer, Berlin. https://doi.org/10.1007/978-3-642-36986-5_2
37. Plestan F, Shtessel Y, Bregeault V, Poznyak A (2010) New methodologies for adaptive sliding mode control. Int J control 83(9):1907–1919
38. Duan G-R, Yu H-H (2013) LMIs in control systems: analysis, design and applications. CRC Press
39. Yu Y, Lu G, Sun C, Liu H (2015) Robust backstepping decentralized tracking control for a 3-DOF helicopter. Nonlinear Dyn. https://doi.org/10.1007/s11071-015-2209-8